

## Microstructure and Corrosion Behavior of $\text{Ni}_{52}\text{Ti}_{48-x}\text{Co}_x$ Shape Memory Alloys in 1.0 M HCl Solution

Nader El-Bagoury<sup>1,2\*</sup>, Mohammed A. Amin<sup>1,3</sup>, H. Shokry<sup>4,5</sup>

<sup>1</sup> Materials and Corrosion Lab, Chemistry Department, Faculty of Science, Taif University, 888 Hawiya, Saudia Arabia

<sup>2</sup> Casting Technology Lab., Manufacturing Technology Dept., Central Metallurgical Research and Development Institute, CMRDI, P. O. Box 87 Helwan, Cairo, Egypt.

<sup>3</sup> Chemistry Department, Faculty of Science, Ain Shams University, P.O. Box 11566, Abbassia, Cairo, Egypt.

<sup>4</sup> Chemistry Department, Faculty of Applied Science, Umm-Al Qura University, Makkah, Saudia Arabia

<sup>5</sup> Chemistry Department, Faculty of Science, Kafr El-Sheikh University, Kafr El-Sheikh 33516, Egypt

\*E-mail: [nader\\_elbagoury@yahoo.com](mailto:nader_elbagoury@yahoo.com)

*Received:* 19 November 2012 / *Accepted:* 13 December 2012 / *Published:* 1 January 2013

---

The effect of Co addition, as an alloying element, on the microstructure and corrosion behavior of  $\text{Ni}_{52}\text{Ti}_{48-x}\text{Co}_x$  ( $x = 0, 0.5, 1.5,$  and  $4.0\%$ ) shape memory alloys (SMAs) was studied. The microstructure of  $\text{Ni}_{52}\text{Ti}_{48-x}\text{Co}_x$  SMAs consisted of B2 austenite phase as the matrix, and small percentages of B19' martensite phase. In addition, two types of NiTi intermetallic compounds were found in the microstructure. The first one was  $\text{Ti}_2\text{Ni}$  and it can be seen in the all microstructures of the four tested SMAs to an extent depending on Co content in the tested SMA. The other type of NiTi precipitates was  $\text{Ni}_2\text{Ti}$ , which found only in the microstructure of  $\text{Ni}_{52}\text{Ti}_{48}\text{Co}_0$  SMA, and completely eliminated upon introducing Co. Tafel polarization and impedance measurements were used to investigate the corrosion behavior of the tested SMAs in 1.0 M HCl solution at 25 °C. The variation with time (up to 24h) of the open circuit potential (OCP) of the tested SMAs was also studied in 1.0 M HCl solution at 25 °C. Results obtained revealed that alloying  $\text{Ni}_{52}\text{Ti}_{48}$  SMA with Co, at the expense of Ti, improved its corrosion resistance. This improvement increased when the percentage of the alloyed Co was increased from 0.5% to 4.0%. The role played by Co in enhancing corrosion resistance of these advanced materials was discussed.

---

**Keywords:** Shape memory alloys; Alloyed Co; Corrosion; Microstructure

## 1. INTRODUCTION

NiTi-based shape memory alloys (SMAs) have attracted much attention because of their potential applications for high temperature conditions (higher than 100 °C), including NiTiX (X=Hf, Zr, thereafter, NiTiX refers to the alloys in which the X is in replacement of Ti) [1], TiNiX (X=Pt, Pd, Au, Si, thereafter, TiNiX refers to the alloys in which the X is in replacement of Ni) alloys [2,3].

Shape memory alloys (SMAs) have the ability to remember a predetermined shape even after severe deformation. Depending on the temperature, a SMA can be austenite, martensite or a mixture of them. Normally, a NiTi SMA transforms between the high temperature B2 phase (austenite, denoted by P) and the low temperature B19' phase (martensite, denoted by M). However, under certain circumstance, which depends on thermal and mechanical effects such as thermal cycling, heat treatment, chemical composition, deformation, etc., an intermediate phase, known as rhombohedral or R-phase (denoted by R), may appear between austenite transforming to martensite, resulting in a two-stage transformation [4,5].

Among currently available shape memory alloys (SMAs), NiTi alloys have superior mechanical properties [6,7]. These alloys have been utilized for selected in vivo applications due to their shape memory effect and superelasticity over the past two decades. These NiTi SMAs also constitute an interesting group of smart alloys which enjoy an ever increasing market share as biomaterials. They are most widely used as orthodontic arch wires, stents, etc.

On the other hand, there have been a number of reports associated with the susceptibility of NiTi alloys to corrosion [8-21]. Khalil-Allafi et al. [22] studied the corrosion behavior of a NiTi SMA with a nominal composition of 50.7 atom% Ni in two physiological environments of Ringer solution and NaCl 0.9% solution. Their experimental findings revealed that the breakdown potential of the NiTi alloy in NaCl 0.9% solution is higher than that in Ringer solution. Authors also reported that, based on topographical evaluations, the corrosion products are nearly same in all samples. The authors in [22] concluded that the NiTi shape memory alloy is not toxic in the physiological environments simulated with body fluids.

Sun et al. [23] investigated the corrosion behaviors of porous and dense NiTi shape memory alloys with the same nominal composition in a 0.9% aqueous NaCl solution using electrochemical methods. The results obtained by Sun et al. indicated that the porous NiTi alloy was more susceptible to localized corrosion than was the dense NiTi alloy. However, the porous NiTi alloy sample with a higher porosity did not suffer more serious corrosion than the one with a lower porosity.

NiTi alloys are attractive materials that are used for medicine. However, Ni-release may cause allergic reactions in an organism. The Ni-release rate is strongly affected by the surface state of the NiTi alloy that is mainly determined by its processing route. In the study of Vojtěch et al. [24], a NiTi shape memory alloy (50.9 at.% Ni) was heat-treated by several regimes simulating the shape setting procedure, the last step in the manufacture of implants. The authors used heating temperatures between 500 and 550 °C and durations from 5 to 10 min. Vojtěch et al. demonstrated that the purpose of the treatments was to obtain and compare different surface states of the Ni-Ti alloy.

The authors in [24] investigated the surface state and chemistry of heat-treated samples by electron microscopy, X-ray photoelectron spectroscopy and Raman spectrometry. Vojtěch et al. taken

the amount of nickel released into a model physiological solution of pH 2 and into concentrated HCl as a measure of the corrosion rate. It was found that the heat treatments produced surface TiO<sub>2</sub> layers measuring 15–50 nm in thickness that were depleted in nickel. The sample covered by the 15-nm thick oxide that was treated at 500 °C/5 min in a low pressure air showed the best corrosion performance in terms of Ni-release. As the oxide thickness increased, due to either temperature or oxygen activity change, Ni-release into the physiological solution accelerated. This finding is discussed in relation to the internal structure of the oxide layers.

Recently [25], we have studied the effect of Re (as an alloying element) on the localized corrosion behaviour of three selected (Ti<sub>51</sub>Ni<sub>49-x</sub>Re<sub>x</sub>) shape memory alloys, x = 0, 0.1, and 0.3%, in aerated neutral 0.05 M KBr solution. Measurements were conducted based on cyclic polarization measurements and showed that the presence of Re enhanced the pitting corrosion resistance of the tested alloys to an extent depending on its content.

Although many research projects have been recently conducted on the corrosion behavior of NiTi SMAs, as we previously clarified, the data are far from sufficient, particularly the corrosion resistance of the Co-NiTi containing SMAs. Little seems to be published concerning the effect of Co as an alloying element on the corrosion behavior of NiTi SMAs.

Phukaoluan et al. [26] studied the effect of Cu and Co additions on corrosion behavior of NiTi shape memory alloys for orthodontic application. The corrosion behavior was assessed electrochemically in artificial saliva (pH 5.35) at 37°C. The results of A. Phukaoluan et al. showed that by adding Co and Cu into NiTi alloys, the corrosion potential ( $E_{\text{corr}}$ ) and the pitting corrosion potential ( $E_{\text{pit}}$ ) increase resulting in improved corrosion resistance.

The work reported herein, and in a continuation of our previous study [25], was undertaken to examine the effect of Co addition (0.5-4.0%), as an alloying element at the expense of Ti, on the uniform corrosion behaviour of Ni<sub>52</sub>Ti<sub>48</sub> SMA in 1.0 M HCl solution. Open circuit potential vs. time, Tafel polarization and impedance measurements were applied in this study.

It was also the purpose of the present work to study the effect of Co addition on the microstructure properties of the tested NiTi SMA.

## 2. EXPERIMENTAL

Ni<sub>52</sub>Ti<sub>48-x</sub>Co<sub>x</sub> shape memory alloys (x= 0, 0.5, 1.5 and 4.0 Co at%) were manufactured by melting in induction vacuum furnace (purity of elements is higher than 99.99%). These alloys were melted four times to ensure homogeneity and cast into an investment casting ceramic mold. Before pouring of the liquid metal, the mold was preheated to 1000 °C.

These alloys were cast as cylindrical rods for the electrochemical tests. These rods machined carefully and mounted in polyester resin after the electric contact, with special care taken to prevent the presence of crevices. The exposed area was ~ 1.0 cm<sup>2</sup>. Before each run, the samples were wet ground with 600-grit silicon carbide (SiC) paper and finally washed in distilled water, followed by immediate rinsing with absolute ethanol.

All chemical and electrochemical tests were performed in 1.0 M HCl solution, as the corrosive medium, prepared with analytical grade chemicals and doubly distilled water. The solution was naturally aerated and the temperature was held at 25 °C using a temperature control water bath. A conventional electrochemical cell was used, consisting of a platinum counter electrode and Ag/AgCl reference electrode. A Luggin–Haber capillary was also included in the design. The tip of the Luggin capillary is made very close to the surface of the working electrode to minimize IR drop.

The electrochemical cell was connected to a potentiostat; Autolab frequency response analyzer (FRA) coupled to an Autolab Potentiostat/Galvanostat (PGSTAT30) with FRA2 module connected to a personal computer.

Variation of open circuit potential (OCP) with time (up to 24 hrs) and Tafel polarization measurements, in addition to impedance measurements at the corrosion potential were used to study the uniform corrosion behavior of  $\text{Ni}_{52}\text{Ti}_{48-x}\text{Co}_x$  SMAs in 1.0 M HCl.

Tafel plots were recorded in a potential window of about -0.25 to 0.25 V vs.  $E_{\text{corr}}$  at a scan rate of  $0.2 \text{ mV s}^{-1}$ . Electrochemical impedance measurements were carried out in the frequency range 100 kHz–10 mHz with an amplitude of 5 mV. All impedance data were fitted to appropriate equivalent circuits using the computer program EQUIVCRT [27].

Before each run, the open circuit potential of the working electrode was measured as a function of time during 24 hrs. The order of performing electrochemical measurements was: (i) Chronopotentiometry (zero current); OCP vs. time (up to 24hrs), followed by (ii) impedance measurements at  $E_{\text{corr}}$  (non-destructive technique);  $E_{\text{corr}}$  = steady-state potential in the OCP vs. time plots, and finally (iii) Tafel polarization ( $E_{\text{corr}} \pm 0.25 \text{ mV}$ ).

At least three separate experiments were carried out for each run to ensure reproducibility of results. The reproducibility of the polarization curves was good. Values of the various electrochemical parameters derived from the employed electrochemical techniques were found to be reproducible. This good reproducibility was expected since a protracted immersion period (24 h) was undertaken to achieve a steady corrosion potential.

The specimens for microstructure examination were prepared by standard metallographic procedures according to standard ASTM: E3-11 then etched in a solution of  $\text{HNO}_3$ , HF and  $\text{H}_2\text{O}$  in a ratio of 4:1:5, respectively. The different phases existing in the structure were analyzed using energy dispersive X-ray spectrometry (EDS) attached in an Analytical Scanning Electron Microscope JEOL JSM 6390 LA, operated at 20 kV.

### 3. RESULTS AND DISCUSSION

#### 3.1. Microstructure

The microstructure of investigated  $\text{Ni}_{52}\text{Ti}_{48}\text{Co}_0$ ,  $\text{Ni}_{52}\text{Ti}_{47.5}\text{Co}_{0.5}$ ,  $\text{Ni}_{52}\text{Ti}_{46.5}\text{Co}_{1.5}$  and  $\text{Ni}_{52}\text{Ti}_{44}\text{Co}_4$  shape memory alloys (SMAs) is shown in Fig. 1.

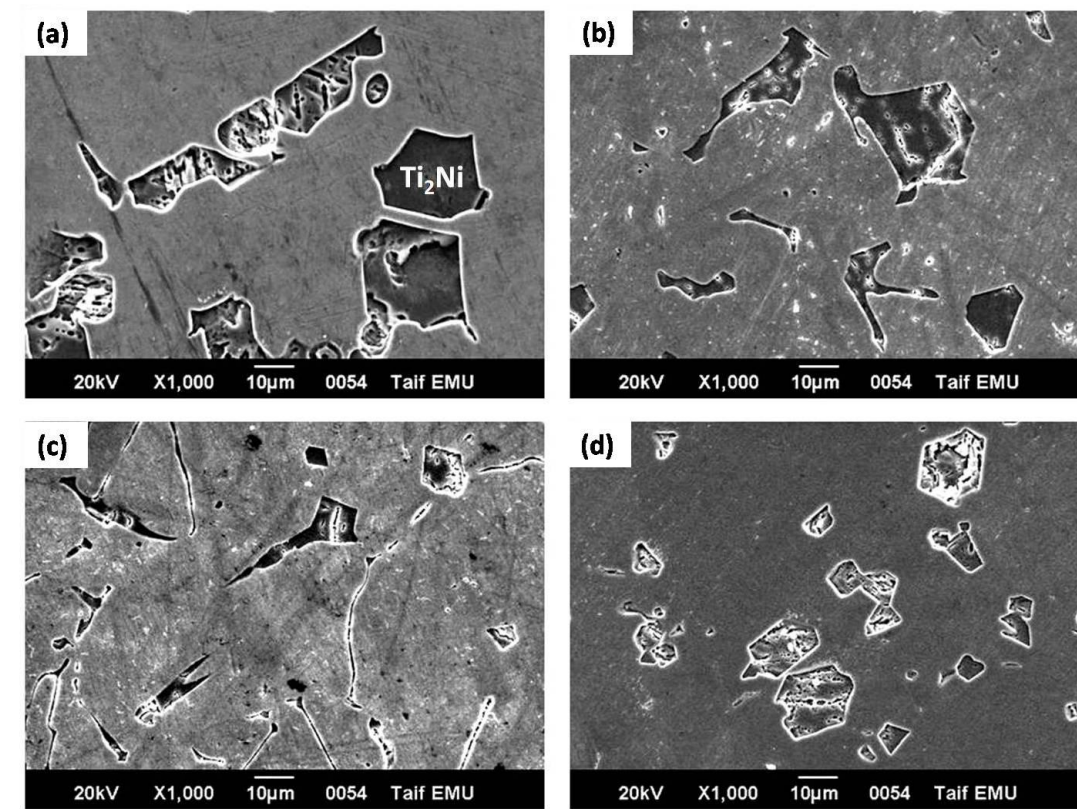


**Figure 1.** Microstructure of the four tested Ni<sub>52</sub>Ti<sub>48</sub>Co<sub>x</sub> SMAs. (a) Ni<sub>52</sub>Ti<sub>48</sub>Co<sub>0</sub> alloy; (b) Ni<sub>52</sub>Ti<sub>47.5</sub>Co<sub>0.5</sub> alloy; (c) Ni<sub>52</sub>Ti<sub>46.5</sub>Co<sub>1.5</sub> alloy; (d) Ni<sub>52</sub>Ti<sub>44</sub>Co<sub>4</sub> alloy.

The microstructure of these alloys consists of B2 austenitic matrix and some precipitates of NiTi intermetallic compound. In Ni<sub>52</sub>Ti<sub>48</sub>Co<sub>0</sub> alloy, a martensite phase can be found only in the microstructure of this alloy, but with a small percentage, as shown in Fig. 2.

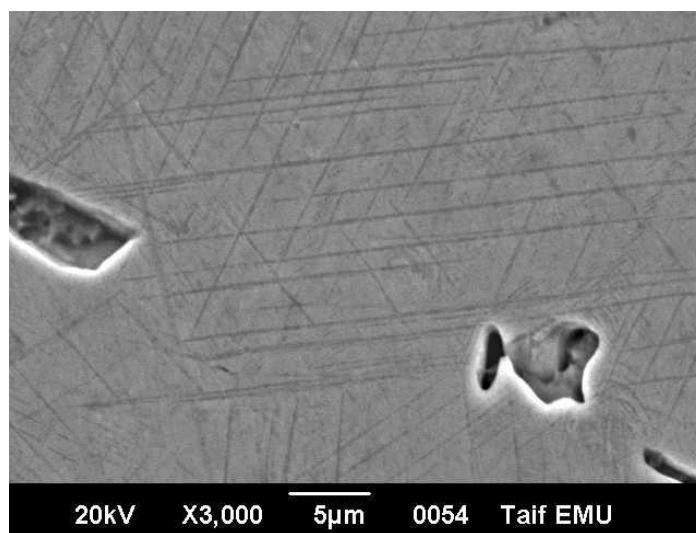


**Figure 2.** Martensite phase in microstructure of Ni<sub>52</sub>Ti<sub>48</sub>Co<sub>0</sub> alloy.

There are two types of NiTi precipitates in the microstructure of such alloys. The first type is the  $Ti_2Ni$  phase, which precipitated in the microstructures of all of the tested SMAs as irregular spherical shapes, Fig. 1. As the Co content increases in SMAs, so does the volume fraction of the  $Ti_2Ni$  phase. The  $Ti_2Ni$  phase is proposed to be one of the main reasons for the increased corrosion resistance of the tested SMAs with increase in Co content (see later).

Upon alloying  $Ni_{52}Ti_{48}$  SMA with Co to yield our tested  $Ni_{52}Ti_{48-x}Co_x$  ( $x = 0, 0.5, 1.5,$  and  $4.0\%$ ) SMAs, Co is found to dissolve mainly in the matrix at the expense of Ti, resulting in an obvious increase in the percentage of  $Ti_2Ni$  phase in the microstructure. On the other hand, the size of this type of precipitates decrease with Co percentage, as shown in Fig. 1.

However, the second type of NiTi precipitates, namely  $Ni_2Ti$  phase are found only in the microstructure of  $Ni_{52}Ti_{48}Co_0$  alloy, as shown in Fig. 3.  $Ni_2Ti$  precipitates are found mainly as small round particles, Fig. 3a, in addition to some of it in a needle-like shape, Fig. 3b.

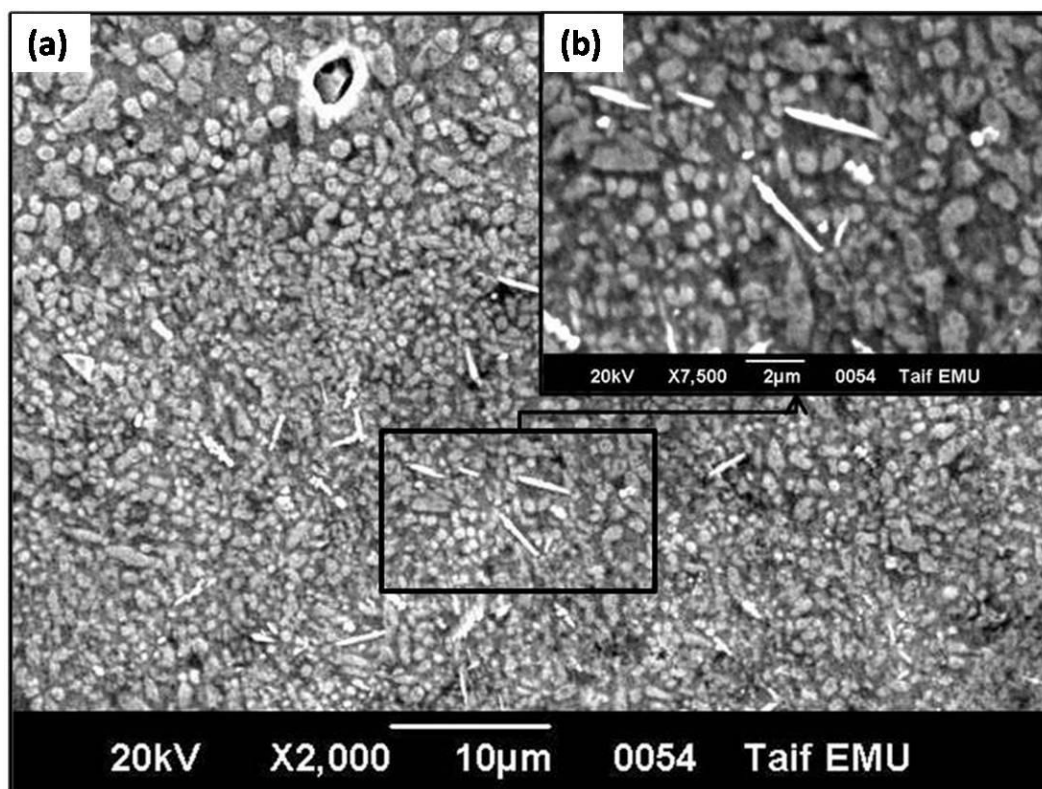


**Figure 3.**  $Ni_2Ti$  precipitates in the microstructure of  $Ni_{52}Ti_{48}Co_0$  alloy. (a)  $Ni_2Ti$  precipitates in small round shape. (b) Higher magnification of the  $Ni_2Ti$  precipitates in needle like-shape.

Some colonies of NiTi phase were found in the  $Ti_2Ni$  precipitates, as shown in Fig. 4. These NiTi colonies sometimes found in a spherical shape, Fig. 4(a), and other times found in irregular rounded shape, Fig. 4(b).



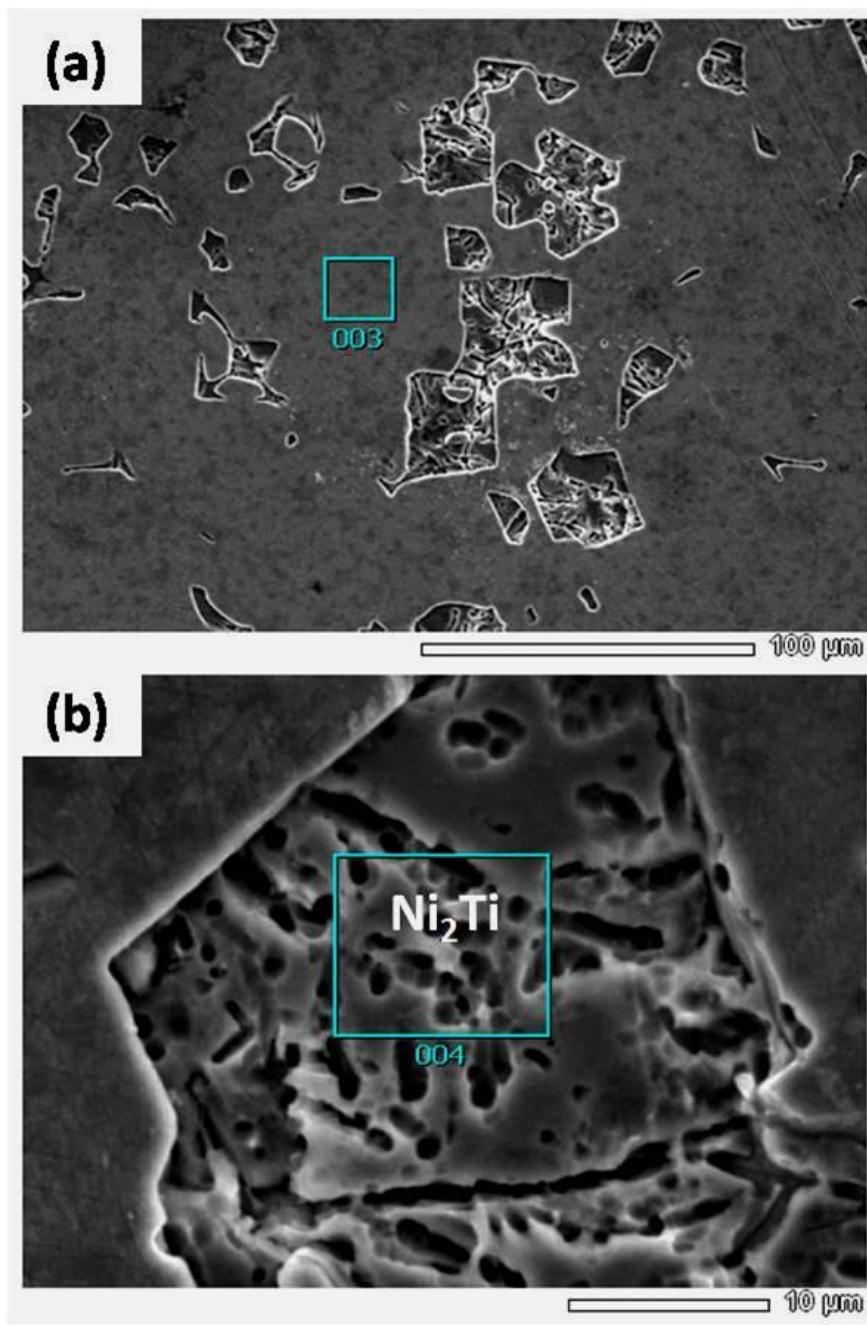


**Figure 5.** Selected positions for EDS analysis for (a) matrix phase and (b)  $\text{Ni}_2\text{Ti}$  phase in  $\text{Ni}_{52}\text{Ti}_{48}\text{Co}_0$  alloy.

It can be noticed that, the matrix has a higher content of Ni than Ti.  $\text{Ni}_2\text{Ti}$  phase is found only in the microstructure of the Co-free SMA ( $\text{Ni}_{52}\text{Ti}_{48}$ ). This phase contains lower Ti contents than Ni, Table 1. This phase did not make, as will be seen later, any benefits for the corrosion resistance for the tested SMAs. On the contrary, its absence is considered to be a great benefit for the corrosion resistance of our testes Co-containing SMAs, see later.

However,  $\text{Ti}_2\text{Ni}$  precipitates have Ti percentage (65%) almost double that of Ni (35%), as shown in Table 1. With increasing Co contents, the contribution of the  $\text{Ti}_2\text{Ni}$  phase is found to significantly increase. On the other hand, upon alloying  $\text{Ni}_{52}\text{Ti}_{48}$  SMA with Co, the  $\text{Ni}_2\text{Ti}$  phase was

completely eliminated from the microstructure of the our tested Co-containing SMAs, corresponding to increased corrosion resistance, see more details in section 3.2.2.

### 3.2. Corrosion behavior of the tested SAMs in 1.0 M HCl

#### 3.2.1. OCP vs. time measurements

The open circuit potentials (OCP) of the four tested SMAs in 1.0 M HCl solution were measured over a period of 24h, as shown in Fig. 6. Potential spikes are observed in such curves, signifying activation and re-passivation processes, i.e., initiation and healing of metastable pits. The magnitude of such spikes decreases when the Co content in the tested alloy increases. This may reflect the passivation influence of the alloyed Co, see later. Similar findings were previously obtained during corrosion of un-welded and welded NiTi SMA in 0.9% NaCl solution [28].

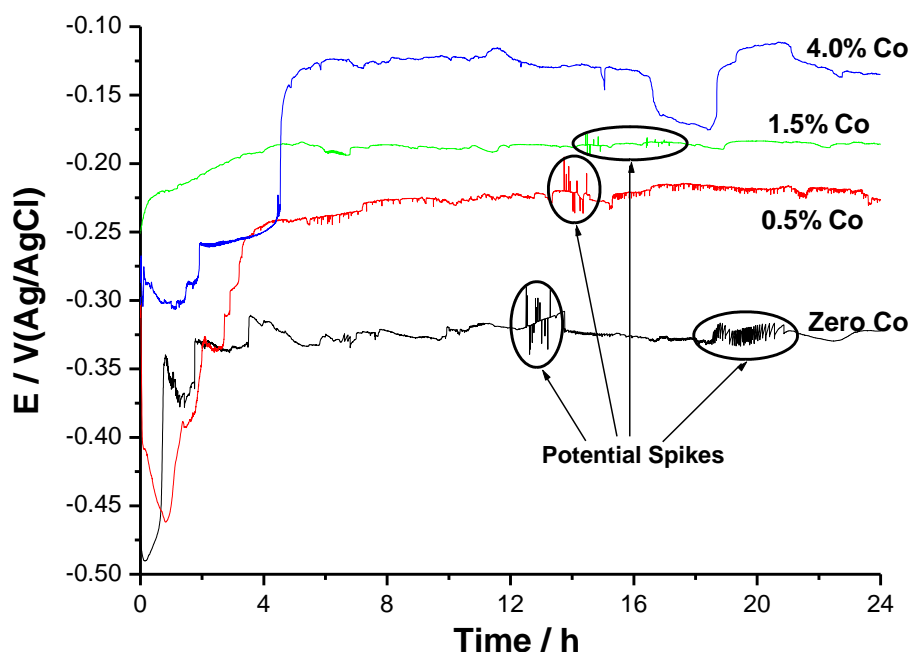


**Figure 6.** Variation with time of the open circuit potentials (OCP) of the four tested SMAs, as a function of Co content, in 1.0 M HCl solution at 25 °C.

With increasing immersion times, the open circuit potentials of the four tested SMAs move towards the more positive values and keep a certain constant value (steady potential), depending on the alloy composition. This steady potential corresponds to, as confirmed from Tafel polarization studies (see later), the free corrosion potential ( $E_{\text{corr}}$ ) of the tested alloy. The steady-state OCP (i.e.,  $E_{\text{corr}}$ ) is made more positive with increase in Co content.

The ennoblement of the open circuit potential observed in Fig. 1 could be generally attributed to healing of the pre-immersion air-formed oxide film and further thickening of the oxide film as a

result of the interaction between the electrolyte and the alloy surface. These findings indicate that the tested alloys tend to passivate in 1.0 M HCl solution to an extent depending on Co% in the tested alloy.

Despite the tendency of the Co-free SMA (i.e.,  $\text{Ti}_{50}\text{Ni}_{50}$  alloy) to passivate in HCl solution, its steady-state OCP value is always more negative than the steady-state OCP values recorded for the other tested SMAs (i.e.,  $\text{Ti}_{50}\text{Ni}_{50-x}\text{Co}_x$  SMAs;  $x = 0.5, 1.5, \text{ and } 4.0\%$  Co). This undoubtedly reflects a more active corrosion surface of the Co-free SMA when compared with the other tested SMAs that alloyed with Co. This difference could be related again to the passivation influence of the alloyed Co. The more positive steady-state OCP values of the three tested SMAs that alloyed with Co also suggests that the presence of the alloyed Co influences the kinetics of the anodic reaction to an extent depending on Co content, as confirmed from Tafel plots (vide infra).

### 3.2.2. Tafel polarization measurements

The effect of the alloyed Co on the nature of the uniform corrosion process of the tested SMAs was also established on the basis of Tafel polarization measurements. Moreover, Tafel polarization measurements were carried out in order to verify the correlation with the OCP vs. time measurements (Fig. 6).

Figure 7 presents the cathodic and anodic polarization plots recorded for the tested SMAs in 1.0 M HCl at a scan rate of  $0.2 \text{ mV s}^{-1}$  at  $25 \text{ }^\circ\text{C}$ .

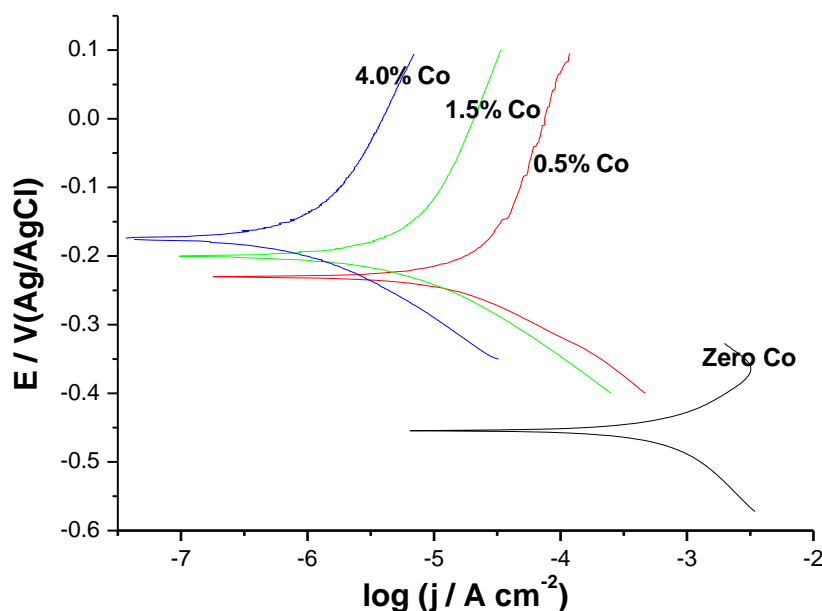


**Figure 7.** Cathodic and anodic polarization plots recorded for the four tested SMAs, as a function of Co content, in 1.0 M HCl solution at a scan rate of  $1.0 \text{ mV s}^{-1}$  at  $25 \text{ }^\circ\text{C}$ .

Generally, the cathodic branch of the polarization curve represents hydrogen evolution, while the anodic one shows alloy dissolution. The various electrochemical parameters, including corrosion potential ( $E_{\text{corr}}$ ), corrosion currents ( $j_{\text{corr}}$ ), anodic Tafel slope ( $\beta_a$ ), and cathodic Tafel slope ( $\beta_c$ ),

associated with such polarization measurements are collected in Table 2 as a function of Co% in the tested alloys.

**Table 2.** Electrochemical parameters derived from Tafel plots (Fig. 7) as a function of alloy composition at 25 °C.

| Type of tested SMA                              | $E_{\text{corr}} / \text{V}(\text{Ag}/\text{AgCl})$ | $j_{\text{corr}} \times 10^4 / \text{A cm}^{-2}$ | $\beta_a / \text{V dec}^{-1}$ | $-\beta_c / \text{V dec}^{-1}$ |
|---|---|--|-------------------------------|--------------------------------|
| $\text{Ni}_{52}\text{Ti}_{48}\text{Co}_0$       | -0.455  | 6.61   | 0.117                         | 0.173                          |
| $\text{Ni}_{52}\text{Ti}_{47.5}\text{Co}_{0.5}$ | -0.231  | 0.33   | 0.089                         | 0.150                          |
| $\text{Ni}_{52}\text{Ti}_{46.5}\text{Co}_{1.5}$ | -0.201  | 0.077  | 0.154                         | 0.132                          |
| $\text{Ni}_{52}\text{Ti}_{44}\text{Co}_{4.0}$   | -0.175  | 0.013  | 0.106                         | 0.129                          |

It is obvious that the cathodic and anodic polarization plots of the tested SMAs are markedly affected by the alloyed Co content. The cathodic and anodic overpotentials increase, the corrosion current densities ( $j_{\text{corr}}$ ) decrease, and the corrosion potential ( $E_{\text{corr}}$ ) moves towards more positive values (in the direction of what was seen by means of OCP vs. time plots, Fig. 6) due to the presence of alloyed Co. These events obviously enhance with the increase in Co content in the sample. Based on these results, the increase of the alloyed Co content enhances the resistance of the alloy towards uniform attack. These findings refer to the passivation influence of the alloyed Co towards uniform corrosion in these solutions.

It is possible that the uniform corrosion process will preferentially dissolve Ni and leave the surface enriched in Co and Ti species (supposed to be un-reactive based on thermo dynamic considerations [29]). The incorporation of Co and Ti species into the passive film may repair the film defects. This greatly reduces the aggressive influence of the corrosive medium (HCl) towards the oxide film, and therefore precludes its significant dissolution.

The improved corrosion resistance of our tested SMAs with increasing Co content can be further explained based on the microstructure and EDS studies presented in section 3.1. Microstructure investigations revealed that alloying with Co our tested SMAs resulted in the formation of intermetallic particles in the solidified structure, namely  $\text{Ti}_2\text{Ni}$  phase.

The existence of  $\text{Ti}_2\text{Ni}$  phase causes a Ti-rich surface layer and a higher Ti/Ni ratio. This will contribute to the improvement in corrosion resistance of the tested NiTi SMAs [30]. Comparing the microstructures of the four tested SMAs, as observed by SEM (Figs. 1-4), many  $\text{Ti}_2\text{Ni}$  precipitates exist in the SMA with the highest Co content (i.e.,  $\text{Ni}_{52}\text{Ti}_{44}\text{Co}_4$  SMA), Fig. 1d, which can cause a higher Ti/Ni ratio on the surface of that alloy and are beneficial to the enhancement of its corrosion resistance. This point will be properly presented and fully discussed in a separate complementary paper.

3.2.3. Impedance measurements

The effect of the addition of Co (as an alloying element) on the complex-plane impedance (Nyquist) plots of Ni<sub>52</sub>Ti<sub>48</sub> SMA has been studied in 1.0 M HCl solution at the respective corrosion potentials at 25 °C. The obtained results are depicted in Fig. 8.

In all cases, the Nyquist plots are characterized by a depressed capacitive time constant, which is the result of the fast charge-transfer process in the alloy dissolution reaction in the HCl solution. The diameter of this time constant is a function of alloy composition (i.e., on Co% in the tested alloy). It can be seen that the overall impedance of the system increases with Co content, which indicates that the electrode surface gets more protection against uniform corrosion in HCl solutions.

The equivalent circuit proposed to fit the experimental data is shown in Fig. 9. It consists of solution resistance  $R_s$  connected with one time constant (i.e., RC circuit). This time constant is composed of the charge-transfer resistance,  $R_{ct}$ , and the constant phase element, CPE.

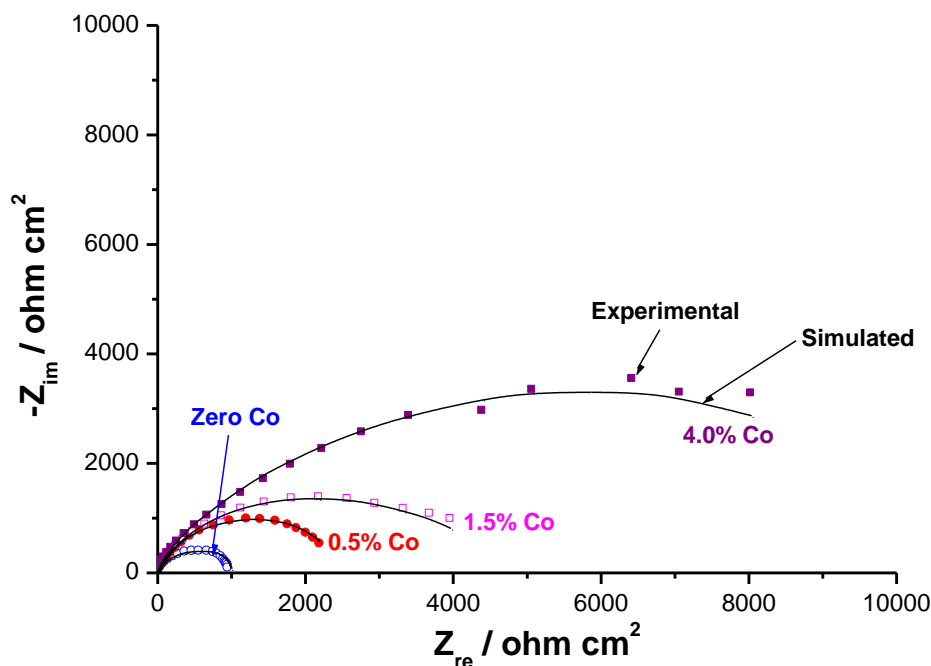


**Figure 8.** Complex-plane impedance (Nyquist) plots recorded for the four tested SMAs, as a function of Co content, in 1.0 M HCl solution at the respective corrosion potentials at 25 °C.

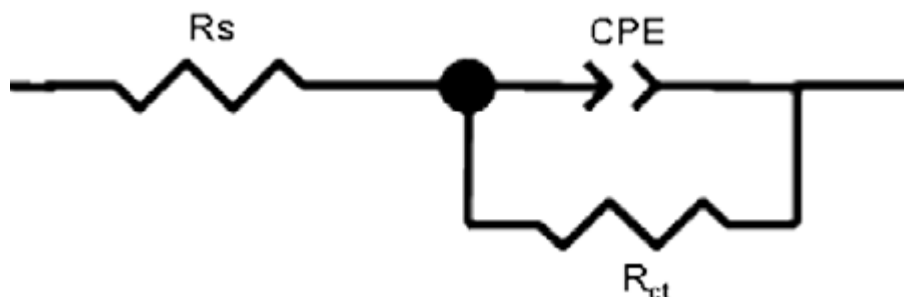


**Figure 9.** The equivalent circuit used to fit and analyze the experimental impedance data.

As can be seen, the constant phase element (CPE) replaces the capacitive element in the proposed equivalent circuit. In many cases CPE is used to describe the distribution of relaxation times, as a result of inhomogeneities present at the solid/liquid interface on a microscopic level (like surface inhomogeneity, roughness, adsorption, formation of porous layers, and variation in properties or compositions of surface layer) [31–37]. Its impedance,  $Z_{CPE}$ , is described by Eq. 1 [31]:

$$Z_{CPE} = [Q (j\omega)^n]^{-1} \quad (1)$$

where  $Q$  is the CPE constant (a proportional factor),  $\omega$  the angular frequency (in  $\text{rad s}^{-1}$ ),  $j^2 = -1$  the imaginary number, and  $n$  is the CPE exponent. The above equation provides information about the degree of non-idealibility in capacitive behaviour. The value of  $n$  makes it possible to differentiate between the behaviour of an ideal capacitor ( $n = 1$ ) and of a constant phase element ( $n < 1$ ). Thus, the value of  $n$  can be used as a measure of the surface inhomogeneity [37,38].

The capacitance was calculated from  $Q$  using the equation [38]:

$$C = [Q R_{ct}^{1-n}]^{1/n} \quad (2)$$

The calculated equivalent circuit parameters for the four tested SMAs in 1.0 M HCl solutions at the respective corrosion potentials are presented in Table 3 as a function of Co content.

**Table 3.** Electrochemical parameters derived from impedance measurements, based on the equivalent circuit presented in the insert of Fig. 8, as a function of alloy composition at 25 °C.

| Type of tested SMA                              | $R_s / \Omega \text{ cm}^2$ | $R_{ct} / \Omega \text{ cm}^2$ | $Q / \text{s}^n (\omega^{-1} \text{ cm}^2)$ | $n$  | $C_{dl} / \mu\text{F cm}^{-2}$ |
|---|-----------------------------|--------------------------------|---|------|--------------------------------|
| $\text{Ni}_{52}\text{Ti}_{48}\text{Co}_0$       | 1.17                        | 1052                           | 3.66  | 0.81 | 25.08                          |
| $\text{Ni}_{52}\text{Ti}_{47.5}\text{Co}_{0.5}$ | 1.2                         | 2445                           | 3.21  | 0.84 | 17.7                           |
| $\text{Ni}_{52}\text{Ti}_{46.5}\text{Co}_{1.5}$ | 0.93                        | 4390                           | 2.45  | 0.89 | 7.67                           |
| $\text{Ni}_{52}\text{Ti}_{44}\text{Co}_{4.0}$   | 1.04                        | 11180                          | 2.05  | 0.93 | 4.36                           |

It is well-known that the smaller the charge-transfer resistance, the faster the corrosion rate. The obtained fitting results indicate that the charge-transfer resistances ( $R_{ct}$ ) increased, and hence the rate of corrosion suppressed, with increase in the percentage of the alloyed Co.

The double layer capacitance is usually observed in the low frequency domain, and its value is largely dependent upon the accumulation of charged species at the interface (adsorption of the aggressive  $\text{Cl}^-$  anions in the present case). The double layer capacitance is, in some way, a measure of the film thickness if the whole film is electrically accessible, see Eq. (3) [39]:

$$C = q (d\theta/dE) \quad (3)$$

where  $q$  represents the total amount of charge stored in the passive film, and  $\theta$  is related to the reactions involved during the oxide layer formation at the corrosion potential [40].

According to the plate capacitor model, the oxide film capacitance,  $C$ , is inversely proportional to its thickness,  $d$ :

$$C = \epsilon_0 \epsilon / d \tag{4}$$

where  $\epsilon_0$  is the permittivity of vacuum,  $\epsilon$  is the dielectric constant of the surface film. Although the actual value of the dielectric constant of the surface film is difficult to estimate, a change of  $C$  can be used as an indicator of a change in the film thickness [41].

Assuming that the dielectric constant does not change with the different parameters under investigation, the reciprocal capacitance of surface film,  $C^{-1}$ , will be directly proportional to the thickness of the passive film [41]. This means that  $C^{-1}$  can be taken as a measure for the passive film thickness. The thickness, and hence the resistance of the passive surface film, increases with increase in Co content, as shown in Fig. 10.

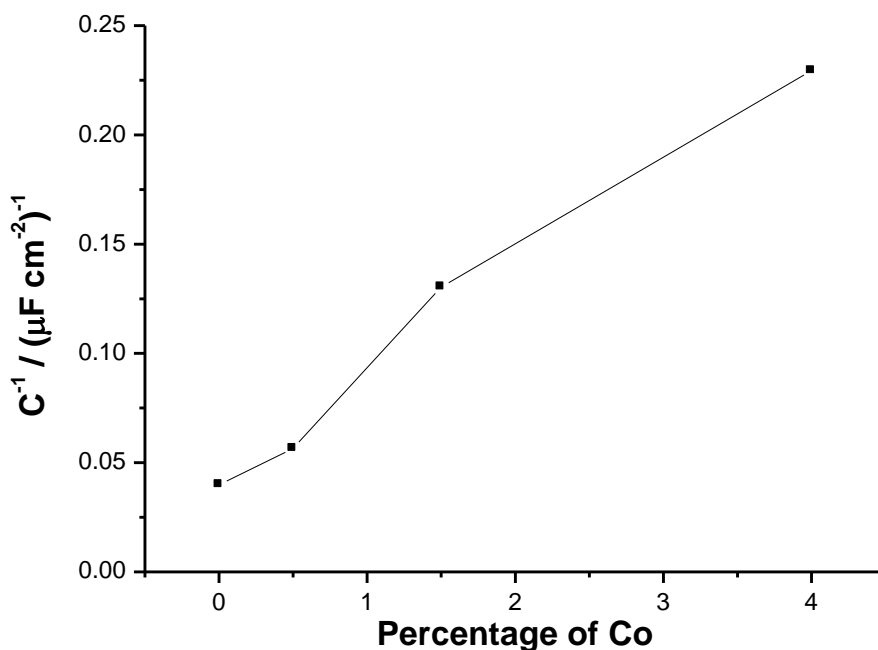


**Figure 10.** Dependence of the reciprocal capacitance,  $C^{-1}$ , of the passive film on percentage of Co in the tested SMA.

These findings indicate a continuous growth of the passive film on the alloy surface with increase in Co content.

Further inspection of Table 3 reveals that the value of  $n$  increases with alloyed Co, indicating a possible increase in surface homogeneities. This additionally pointed to the increase of protective properties of the surface layer with increasing alloyed Co content.

#### 4. CONCLUSIONS

The corrosion behaviour of Ni<sub>52</sub>Ti<sub>48-x</sub>Co<sub>x</sub> (x = 0, 0.5, 1.5, and 4.0%) shape memory alloys (SMAs) in 1.0 M HCl solution was studied by Tafel polarization and electrochemical impedance spectroscopy measurements. The results of corrosion testing and microstructure analyses suggest the following conclusions:

- OCP vs. time measurements showed that with increasing immersion time, the open circuit potentials of the four tested SMAs move towards the more positive values. This means that the four tested SMAs tend to passivate in 1.0 M HCl solution.
- Compared to the Co-free NiTi SMA, the Co-containing SMAs exhibited higher open circuit potentials proportionally to the Co content, corresponding to improved corrosion resistance.
- Tafel polarization measurements showed that the four tested SMAs corrode in 1.0 M HCl solutions, and the corrosion resistance increased with increase in Co% in the tested SMA.
- The results of impedance measurements at open circuit potential have shown that the overall impedance of the system increases with Co content due to continuous growth of a more protective (defect-free) passive film on the alloy surface.
- Microstructures studies revealed that the existence of Ti<sub>2</sub>Ni phase in the Co-containing SMAs (the contribution of such phase enhances with Co content) caused a Ti-rich surface layer and a higher Ti/Ni ratio. This imparted a significant improvement in corrosion resistance of the Co-containing SMAs, as compared with Co-free NiTi SMA.

#### ACKNOWLEDGEMENT

The authors acknowledge the financial aid received from Taif University, Saudia Arabia (Project No. 1/433/1670).

#### References

1. E.K. Eckelmeyer, *Scripta Met.*, 10 (1976) 667.
2. Y.C. Lo, S.K. Wu, C.M. Wayman, *Scripta Met. et Materialia*, 24 (1990) 1571.
3. K.h. M. Ibrahim, N. El-Bagoury, Y. Fouad, *J. Alloys and Compounds*, 509 (2011) 3913.
4. Q. Feng, S. Ping, L. Chang, J. Qichuan, *Mat. and Des.*, 34 (2012) 143.
5. JIANG Shu-yong, ZHANG Yan-qiu, *Trans. Nonferr. Metal. Soc. of China*, 22 (2012) 90.
6. S. Miyazaki and K. Otsuka: *ISIJ Int.* 29 (1989) 353–377.
7. K. N. Melton: Engineering Aspects of Shape Memory Alloys, T. W. Duerig, K. N. Melton, D. Stockel and C. M. Wayman (eds), (Butterworth-Heinemann, New York, 1990) pp. 21–35.
8. N. K. Sarkar, W. Redmond, B. Schwaninger and A. J. Goldberg: *J. Oral Rehabil.* 10 (1983) 121–128.
9. S. Lu: Engineering Aspects of Shape Memory Alloys, T. W. Duerig, K. N. Melton, D. Stockel and C. M. Wayman (eds), (Butterworth-Heinemann, New York, 1990) pp. 445–451.
10. Y. Oshida, R. Sachdeva, S. Miyazaki and S. Fukuyo: *Mater. Sci. Forum* 56–58 (1990) 705–710.
11. D.D. Macdonald, *Pure Appl. Chem.*, 71 (1999) 951.
12. R.P. Frankenthal, J. Kruger (Eds.), Passivity of Metals, *Electrochem. Soc. Princeton, NJ* (1978), p. 165.

13. T.R. Beck, *J. Electrochem. Soc.*, 120 (1973) 1310.
14. T.P. Hoar, *Corros. Sci.*, 5 (1965) 279.
15. J. Kruger, *Int. Mater. Rev.*, 33 (1988) 113.
16. J. Stewart, D.E. Williams, *Corros. Sci.*, 33 (1992) 457.
17. G.S. Frankel, *J. Electrochem. Soc.*, 145 (1998) 2970.
18. S.Y. Yu, W.E. O'Grady, D.E. Ramaker, P.M. Natishan, *J. Electrochem. Soc.*, 147 (2000) 2952.
19. Z. Jiang, X. Dai, T. Norby, H. Middleton, *Corros. Sci.*, 53 (2011) 815.  
*Int. J. Electrochem. Sci.*, Vol. 7, 2012 2653
20. Z. Jiang, T. Norby, H. Middleton, *Corros. Sci.*, 52 (2010) 3158.
21. A.D. Davydov, *Electrochim. Acta*, 46 (2001) 3777.
22. Jafar Khalil-Allafi, B. Amin-Ahmadi, M. Zare, *Materials Science and Engineering: C*, 30 (2010) 1112.
23. X.T. Sun, Z.X. Kang, X.L. Zhang, H.J. Jiang, R.F. Guan, X.P. Zhang, *Electrochim. Acta*, 56 (2011) 6389.
24. D. Vojtěch, M. Voděrová, J. Fojt, P. Novák, T. Kubásek, *Appl. Surf. Sci.*, 257 (2010) 1573.
25. M.A. Amin, N. El-Bagoury, A.A. Omar, A.S. Megahed, *Int. J. Electrochem. Sci.*, 7 (2012) 2643 – 2653.
26. A. Phukaoluan, Anak Khantachawana, S. Dechkunakorn, N. Anuwongnukroh, P. Santiwong, Julathep Kajornchaiyakul, *Advanced Materials Research*, 378 – 379 (2011) 650.
27. B.A. Boukamp, Equivalent Circuit, Princeton Applied Research Corporation, Princeton, NJ, 1990.
28. X.J. Yan, D.Z. Yang, X.P. Liu, *Materials Characterization*, 58 (2007) 623.
29. M. Pourbaix, Atlas of Electrochemical Equilibria in Aqueous Solutions, NACE, Houston, TX, 1975.
30. H.C. Man, Z.D. Cui, T.M. Yue, *Scr. Mater.*, 45 (2001) 1447.
31. I.D. Raistrick, J.R. Macdonald, D.R. Franceschetti, in: J.R. Macdonald (Ed.), Impedance Spectroscopy, J. Wiley & Sons, New York, 1987.
32. J. Hitzig, J. Titz, K. Juttner, W.J. Lorenz, E. Schmidt, *Electrochim. Acta*, 29 (1984) 287.
33. A.E. Bohe, J.R. Vilche, K. Juttner, W.J. Lorenz, W. Paatsch, *Electrochim. Acta*, 34 (1989) 1443.
34. U. Rammelt, G. Reinhard, *Electrochim. Acta*, 35 (1990) 1045.
35. Z. Stoynov, *Electrochim. Acta*, 35 (1990) 1493.
36. A. Popova, E. Sokolova, A. Raicheva, M. Christova, *Corros. Sci.*, 45 (2003) 33.
37. D. Kek-Merl, J. Lappalainen, H.L. Tuller, *J. Electrochem. Soc.*, 153 (2006) J15.
38. G. Lojen, I. Anžel, A. Kneissl, A. Križman, E. Unterweger, B. Kosec, M. Bizjak, *J. Mater. Process. Technol.*, 162–163 (2005) 220.
39. B.E. Conway, Electrochemical Supercapacitors Scientific Fundamentals and Technological Applications, Kluwer Academic Publishers, New York, USA, 1999 (Chapter 10).
40. M.A. Amin, S.S. Abd El-Rehim, E.E.F. El-Sherbini, S.R. Mahmoud, M.N. Abbas, *Electrochim. Acta*, 54 (2009) 4288.
41. M. Gojic, L. Vrsalovic, S. Kozuh, A. Kneissl, I. Anzel, S. Gudic, B. Kosec, M. Kliskic, *J. Alloys and Compounds*, 509 (2011) 9782.